Available online at www.sciencedirect.com
ScienceDirect
Sensors and Actuators B 133 (2008) 118–127
SENSORS AND ACTUATORS B CHEMICAL
www.elsevier.com/locate/snb

Fabricating random arrays of boron doped diamond nano-disc electrodes: Towards achieving maximum Faradaic current with minimum capacitive charging

Lei Xiao, Ian Streeter, Gregory G. Wildgoose, Richard G. Compton *

Department of Chemistry, Physical and Theoretical Chemistry Laboratory, Oxford University, South Parks Road, Oxford OX1 3QZ, United Kingdom

Received 3 December 2007; received in revised form 25 January 2008; accepted 4 February 2008
Available online 9 February 2008

Abstract

We report the first construction of a *random* array of boron doped diamond (BDD) nano-disc electrodes (RAN BDD), formed by a simple three-step method. First molybdenum(IV) dioxide nanoparticles are electrodeposited onto a BDD substrate. Second the electrode surface is covered in an insulating polymer film by the electropolymerization of a 4-nitrophenyldiazonium salt. Third the molybdenum dioxide nanoparticles are dissolved from the BDD surface (removing the polymer layer directly above them only) using dilute hydrochloric acid to expose nano-discs of BDD, *ca.* 20 ± 10 nm in diameter surrounded by a polymer insulating the remainder of the BDD. This method produces up to 650 ± 25 million BDD nano-disc electrodes per cm^2. Various RAN BDD electrodes were produced using this method with a similar distribution of nano-disc size and number density, confirming that this is a reliable and reproducible method of manufacturing such nanoelectrode arrays.

At modest scan rates the RAN BDD array was found to produce peak currents approaching that of the Randles–Ševčík limit for the equivalent geometric electrode area despite the fact that most of the surface was insulated by the polymer as shown by voltammetry and atomic force microscopy. The experimental results are compared with simulations of both ordered and random arrays of nano-disc electrodes, the results of which demonstrate that the maximum current obtainable at such arrays is that predicted by the Randles–Ševčík equation. The array of BDD nano-discs shows a significantly reduced capacitive background current compared to the bare BDD electrode, suggesting that such devices may offer improved signal resolution in electroanalytical measurements.
© 2008 Elsevier B.V. All rights reserved.

Keywords: Boron doped diamond; Nanoelectrode; Random array; Voltammetry; Atomic force microscopy; Diffusion

1. Introduction

The Nobel Laureate Hubel is widely credited with inventing the first, modern day, metal microelectrode over 50 years ago [1]. Since then, microelectrodes have been routinely used in analytical and physiological applications due to their many advantageous properties. These include low background charging currents, large current density due to convergent diffusion to the microelectrode, small size and sample volume, low depletion of the target analyte and the ability to be used in highly resistive media in a two-electrode, as opposed to a conventional three-electrode, arrangement without requiring a supporting electrolyte [2]. The beneficial properties of using a single microelectrode can often be enhanced by the use of either an ordered or random array of microelectrodes.

The behavior of such an array strongly depends on the degree to which each microelectrode element in the array is diffusionally independent from the other elements. This in turn depends on both the separation of each microelectrode in the array relative to the diameter of the individual microelectrodes, and also the timescale of the voltammetric experiment [3–6]. If the electrodes within the array are sufficiently separated, and the timescale of the experiment is short enough that the diffusion layers that develop around each microelectrode do not overlap, then each electrode within the array can be considered to be diffusionally independent from its neighbors (see Scheme 1) [7–10].

The limit of extreme overlapping of diffusion zones occurs when the distance of separation between electrodes is small, or when the timescale of the experiment is longer. In this limit

* Corresponding author. Tel.: +44 1865 275413; fax: +44 1865 275410.
E-mail address: richard.compton@chem.ox.ac.uk (R.G. Compton).

0925-4005/$ – see front matter © 2008 Elsevier B.V. All rights reserved.
doi:10.1016/j.snb.2008.02.003

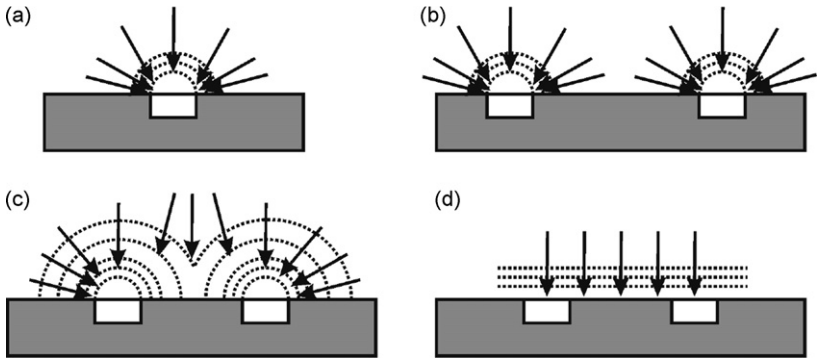

Scheme 1. (a) Convergent diffusion to an individual microelectrode. (b) Convergent diffusion to neighboring microelectrodes within an array that are sufficiently spaced at short voltammetric time scales so as to remain diffusionally independent (type II behavior). (c) The same neighboring electrodes at longer voltammetric time scales where the inter-disc separation is no longer sufficient to prevent overlap of the diffusion layers surrounding each microdisc—a diffusionally quasi-independent array (type III behavior). (d) The same two neighboring electrodes at sufficiently long voltammetric time scales that their diffusion layers are fully overlapping and diffusion to the electrodes is now planar, not convergent (type IV behavior).

a diffusion layer is formed which has uniform thickness over the whole array [5]. The current measured is therefore equal to that predicted by a planar diffusion model, and the peak current of a voltammogram recorded in this limit is given by the Randles–Ševčík equation [2]:

$$i_p = 2.69 \times 10^5 n^{3/2} D^{1/2} C_{bulk} \nu^{1/2} A \quad (1)$$

where n is the number of electrons transferred, D is the diffusion coefficient ($cm^2\ s^{-1}$), C_{bulk} is the bulk concentration of the analyte ($mol\ cm^{-3}$), ν is the scan rate ($V\ s^{-1}$) and A is the electrode area (cm^2). The Randles–Ševčík peak current represents the maximum possible peak current that can be recorded at a microdisc array; further increases in the number of discs present cannot enhance the current since there is already maximum overlapping of neighboring diffusion zones.

There exist in the literature a variety of methods of fabricating arrays of metal nanoelectrodes on electrode surfaces, such as electrochemical or electroless deposition of metal nanoparticles onto a suitable electrode substrate [9,10]. These methods produce random arrays of nanoparticles on the electrode surface, such that the array rarely, if ever, is diffusionally independent on most practical experimental timescales. Lithographic techniques of fabricating ordered micrometer and nanometer sized metal arrays are progressing, such as the use of ion-beam milling [11,12] and/or nanoimprinting [13], but these techniques are limited in that they can only produce nanoelectrodes with diameters of the order of 100 nm, whilst a significant fraction of the individual electrodes in the array are not in electrical contact with the substrate, forming "dead" electrodes [14].

Conducting forms of carbon, including graphite, glassy carbon, carbon nanotubes and boron doped diamond (BDD) have been shown to have desirable properties as electrode substrates for electroanalysis of a wide range of analytes [15]. The fabrication of carbon microelectrode arrays is somewhat more difficult than for metal microelectrode arrays due to the intrinsic mechanic properties of these forms of carbon. Methods of making graphitic microelectrode arrays can be found in the literature, however if graphite itself is used as the substrate the fabrication process is often involves chemical or thermal vapor deposition, plasma etching or lithographic techniques which prohibit their widespread applicability [15,16]. One simple method of constructing random arrays of carbon microelectrodes (RAM), developed by Fletcher and Horne [17], is to seal carbon fibers in a suitable insulator such as epoxy resin, and these types of electrodes have been used in analysis to great effect [18–23].

Constructing arrays of carbon nanoelectrodes has proved yet more difficult. Vertically aligned arrays ("forests") of multiwalled carbon nanotubes (MWCNTs) have been studied by numerous researchers [24–29], and are now commercially available [30], but sealing them effectively in an insulating layer is not facile. One notable example is the work of Li et al. who have developed a method of constructing a random array of closely spaced MWCNTs sealed in a silicon oxide insulating material, and applied this system to the electroanalysis of DNA and various other analytes [31–33].

BDD consists of sp^3 hybridized carbon in a diamond lattice structure, where approximately one carbon atom in a thousand is replaced by an atom of boron. This imparts electrical conductivity to the material, which is one of the most attractive carbon substrates for electroanalysis due to the large potential window (up to 3 V in aqueous electrolyte solutions), low background current, mechanical durability and resistance to surface fouling [34]. However, the doping levels, and hence conductivity, of BDD crystals has been shown to be spatially heterogeneous, leading to significant fractions of the electrode surface being non-conductive [35]. These "dead" zones on the BDD surface significantly reduce the electrode's electroanalytical performance, particularly in terms of achieving the maximum possible peak currents and hence lowest detection limits and sensitivities to target analytes. To the best of the authors' knowledge only five reports exist in the literature using ordered and random BDD microelectrode arrays, mainly due to the diffi-

culty in making them [34,36–39]. To date there are no reports on the fabrication of BDD nanoelectrodes or nanoelectrode arrays.

Previous work in our own laboratory has developed a method of fabricating random arrays of nanobands or "nanotrenches" along the edge-plane step defects on a highly ordered pyrolytic graphite (HOPG) surface [40,41]. This method is a development of the work of Penner and co-workers [42,43] who found that nanowires of molybdenum dioxide could be electrodeposited selectively along edge-plane step defects on graphite. In this report we describe, for the first time, the formation of a random array of BDD nano-disc electrodes using a similar method to that used previously to form the nanobands on graphite [40,41]. Quasi-hemispherical nanoparticles of molybdenum dioxide (MoO_2) are electrodeposited onto a BDD substrate. The electrode is then covered in an insulating film via the electropolymerization of a 4-nitrophenyldiazonium salt. Finally the MoO_2 nanoparticles are dissolved using aqueous hydrochloric acid, removing the polymer film above them (see Scheme 2) but not the surrounding polymer. This results in the formation of 650 million nano-discs of BDD per cm^2, *ca.* 20 nm in diameter. The random array of BDD nano-discs (RAN BDD) is characterized using cyclic voltammetry and atomic force microscopy (AFM).

The size and spacing between neighboring BDD nano-discs within the RAN BDD array is such that the diffusion layers surrounding each individual element (BDD nano-disc) overlap to a substantial degree at modest scan rates. As such diffusion to the RAN BDD electrode is considered to be planar. This results in "macrodisc-like" voltammetric behavior where the maximum obtainable peak current at the RAN BDD array is the Randles–Ševčík limit for the geometric area of the entire array. This is despite the fact that most of the electrode surface is covered by insulating polymer and only a tiny fraction of the electrode surface is therefore electroactive. Furthermore because only a fraction of the RAN BDD electrode surface is electroactive the capacitive charging (background) current is significantly reduced compared to the bare BDD macrodisc. The current enhancement observed at RAN BDD electrodes has significant potential for use in electroanalysis and detection of trace analytes.

2. Experimental

2.1. Reagents and equipment

All reagents obtained from Aldrich (Gillingham, UK) with the exception of: anhydrous acetonitrile and hydrochloric acid (37%, v/v) (Fisher Scientific, Loughborough, UK), tetrabutylammonium perchlorate (TBAP, >99%, Fluka, Dublin, Ireland), 4-nitrobenzenediazonium tetrafluoroborate (Acros Organic, Loughborough, UK), potassium ferrocyanide ($K_4Fe(CN)_6$, Lancaster, Morecamble, UK) and were of the highest commercially obtainable grade and used without further purification. Aqueous solutions were prepared using deionized water from a Vivendi UHQ grade water system (Millipore, UK) with a resistivity of not less than 18.2 MΩ cm at 25 °C.

Electrochemical measurements were recorded using a type III μAutolab computer controlled potentiostats (Ecochemie, Utrecht, The Netherlands) with a standard three-electrode setup. A boron doped diamond (BDD, 3 mm diameter, Windsor Scientific, Slough, UK) electrode acted as the working electrode with the cell assembly being completed by a platinum wire (99.99%, GoodFellow, Cambridge, UK) counter electrode and a saturated calomel electrode (SCE, Radiometer, Copenhagen, Denmark) reference electrode. The unmodified BDD electrode was successively polished using diamond spray (Kemet, UK) with particle sizes of 3.0, 1.0, and 0.1 μm prior to use. The BDD electrode was sonicated in pure water for 5 min and rinsed with ethanol between successive polishing to remove any diamond particles from the electrode surface. Voltammetric experiments were performed at 20 ± 2 °C in electrolyte solutions that were degassed with pure N_2 gas (BOC, Guildford, UK) for fifteen minutes prior to use.

Atomic force microscopy (AFM) measurements were performed using a Digital Instruments Multimode SPM (Veeco, New York, USA) operating in *ex situ* tapping mode. A model J scanner was used having a lateral range of 125 μm × 125 μm and a vertical range of 5 μm.

3. Results and discussion

The fabrication of the RAN BDD array was monitored using both cyclic voltammetry and AFM. Fig. 1a shows the resulting voltammetry at a scan rate of 100 mV s^{-1} at the bare (unmodified) BDD electrode in a solution of 1.0 mM potassium ferrocyanide containing 0.1 M KCl as supporting electrolyte. The observed voltammetry exhibits oxidative and reductive peak currents centered at *ca.* +0.2 V vs. SCE in a 1:1 ratio, separated by *ca.* 100 mV. This indicates that the redox behavior of ferrocyanide at the BDD electrode exhibits fast (quasi-reversible) electrode kinetics at the macroelectrode. The scan rate was varied from 10–10,000 mV s^{-1} and produced a linear relationship between the peak current and the square root of scan rate, as expected for a redox active species diffusing in solution.

Next molybdenum dioxide (MoO_2) nanoparticles were electrochemically deposited onto the BDD electrode from a solution of 1.1 mM sodium molybdate(VI) (Na_2MoO_4), 1.0 M NaCl and 1.0 M NH_4Cl adjusted to pH 8.48 with 1 M NH_4OH. The electrode was held at a potential of −1.0 V vs. SCE for five seconds. This method was adapted from the work of Penner et al. [42,43] and has been used in this laboratory to decorate the edge-plane-like defects on the surface of graphite and MWCNTs to form nanobands [40,41] and nanoplugs of MoO_2 on these surfaces, respectively [44]. The electrodeposition step occurs by the reaction shown in Eq. (2):

$$MoO_4^{2-} + 2H_2O + 2e^- \rightarrow MoO_2 + 4OH^- \quad (2)$$

After electrodepositing the MoO_2 nanoparticles the electrode was washed with pure water and allowed to dry in an oven at 40 °C for several hours prior to examination using AFM. Fig. 2a and b show the AFM images recorded before and after deposition

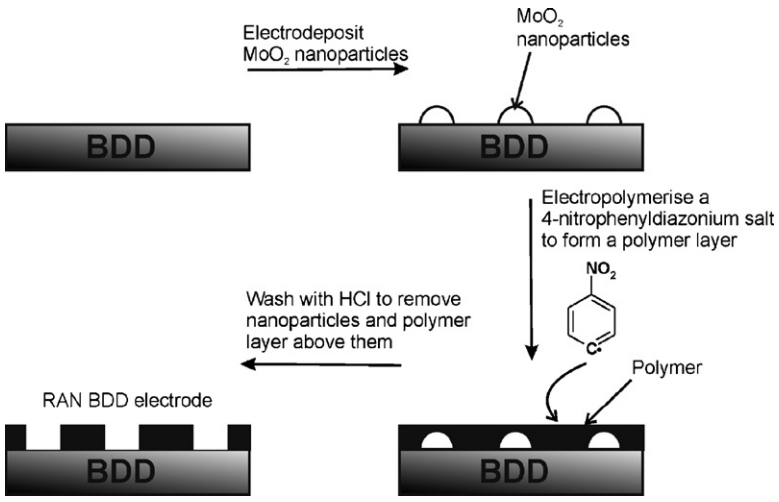

Scheme 2. A cartoon showing the three-step process to fabricate the RAN BDD electrode.

of the MoO_2 nanoparticles. Before deposition a smooth, clean BDD surface is observed. The optimal deposition potential of −1.0 V vs. SCE and deposition time of five seconds produced a random array of quasi-hemispherical nanoparticles of MoO_2, 10–200 nm in diameter and 20–100 nm in height as shown in Fig. 2b.

Cyclic voltammetry was again performed in the same 1.0 mM solution of ferrocyanide using the MoO_2 nanoparticle modified BDD electrode over a range of scan rates from 10 mV s^{-1} up to 10 V s^{-1}. Fig. 1b shows the resulting voltammetry at a scan rate of 100 mV s^{-1} for comparison. Almost identical voltammetry is observed to that at the bare BDD electrode, with similar peak cur-

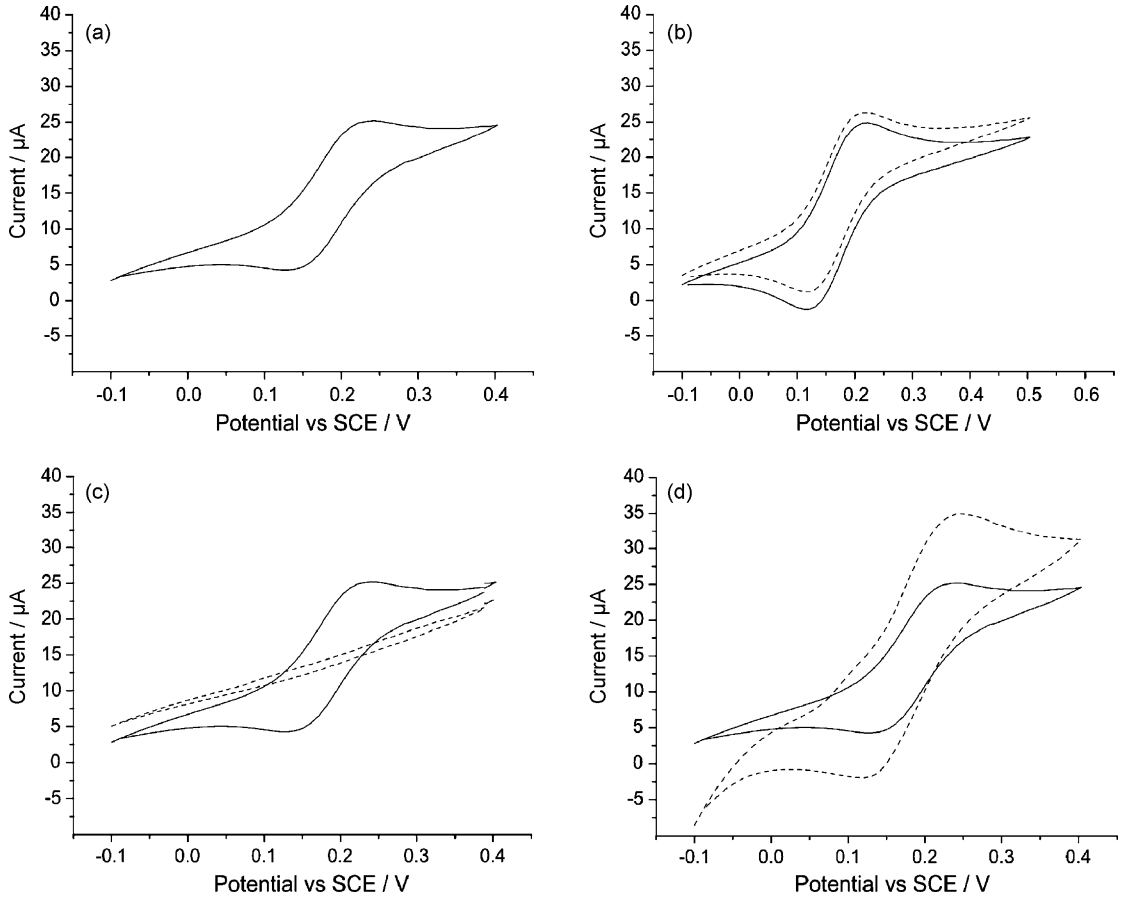

Fig. 1. The cyclic voltammetric response (scan rate 100 mV^{-1}) of a 1.0 mM solution of potassium ferrocyanide at: (a) the bare BDD electrode, (b) the MoO_2 nanoparticle modified BDD electrode (solid line) compared to the response at the bare BDD electrode (dashed line); (c) the polymer film covered electrode (dashed line) compared to the bare BDD electrode (solid line); (d) the RAN BDD electrode (dashed line) compared to the bare BDD electrode (solid line).

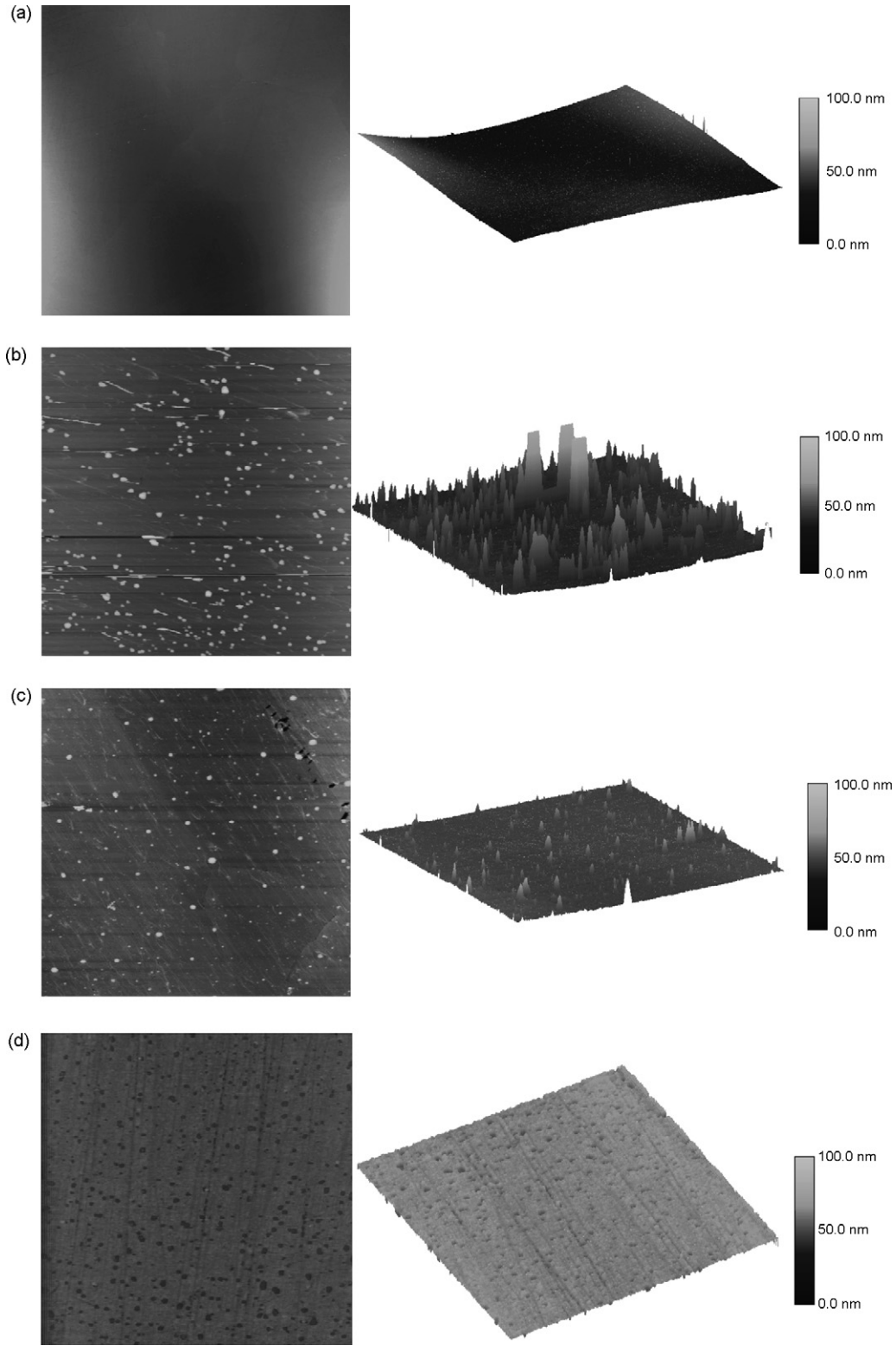

Fig. 2. AFM images showing the 2D (left) and 3D (right) surfaces of: (a) the bare BDD electrode; (b) the MoO_2 nanoparticle modified electrode; (c) the polymer film covered electrode; (d) the RAN BDD electrode.

rents and potentials observed. Note that the MoO_2 nanoparticles are electrically conducting, however the electron transfer kinetics are likely much slower at the MoO_2 nanoparticles compared to the BDD substrate [40,41]. Due to the size and dispersion of the random array of nanoparticles on the surface, the electrode can be considered as a partially blocked electrode [3,4,45,46], with the MoO_2 nanoparticles acting as the blocking material. Because the radii of the blocks are small compared to their separation on the electroactive BDD surface, redox active material is able to diffuse over the "blocks" on the voltammetric

timescale. Thus the voltammetry is dominated by the faster electron transfer at the BDD surface, and the presence of the MoO_2 nanoparticles is voltammetrically innocuous. This effect is treated theoretically in more detail elsewhere [3,4,45,46].

Previously, members of our research group have created "nanotrenches" along the edge-plane defect sites on a highly ordered pyrolytic graphite (HOPG) electrode by covering the electrode surface in an insulating polymer layer, formed by reductive electrolysis of 4-nitrobenzenediazonium tetrafluoroborate [41]. The polymer layer grows over both the HOPG surface and the MoO_2 nanobands which were electrodeposited onto the edge-plane defect sites. Treatment with dilute hydrochloric acid then dissolves the MoO_2, taking with it the polymer on top of the nanobands, but leaves the polymer over the HOPG surface intact.

To see if we could adapt this method to create a random array of BDD nanodiscs on the electrode surface, the MoO_2 nanoparticle modified electrode was coated in the insulating polymer in the same fashion. To this end the modified electrode was immersed in a 1.2 mM solution of 4-nitrobenzenediazonium tetrafluoroborate in acetonitrile containing 0.1 M TBAP as supporting electrolyte. A potential of −0.5 V vs. Ag was applied to the working electrode for a period of eighty seconds, after which time the electrode was rinsed with acetonitrile to remove any unreacted species and electrolyte salt and left to air dry. The 4-nitrobenzenediazonium salt is reduced at this potential in a one-electron step forming a 4-nitrophenyl radical and dinitrogen gas. The 4-nitrophenyl radical then undergoes polymerization on the electrode surface, to form the insulating polymer layer.

Fig. 1c shows the resulting voltammetric response of the polymer coated BDD electrode in the ferrocyanide solution. No voltammetry can be observed corresponding to the redox chemistry of ferrocyanide, indicating that the electrode surface is completely blocked by the insulating polymer. Fig. 2c shows the resulting AFM image of the polymer coated electrode. The polymer layer was found to be between 5 and 20 nm in height and covers the entire electrode surface. Only the very largest of the MoO_2 nanoparticles (covered in polymer) can be observed above the polymer layer, with the smaller nanoparticles completely covered up.

Finally, the MoO_2 nanoparticles were removed from the electrode surface (taking the polymer above them with them) by immersing the polymer coated BDD electrode in 30 cm^3 of 2.0 M aqueous HCl and stirring the solution for 10 min to form a random array of nano-disc BDD electrodes. The electrode surface was again examined with AFM as shown in Fig. 2d. A random array of circular holes, *viz.* BDD nano-discs, with a depth of 10–20 nm was formed in the polymer film, revealing the BDD substrate beneath. The size of the nano-discs was determined from the AFM image using a line segment analysis across a sample of two hundred nano-discs as shown in Fig. 3. A normal distribution of diameters was observed with a mean diameter of 20 nm (standard deviation, σ, ±10 nm). A very small number (<2%) of BDD nano-discs had diameters as large as 200 nm. From Fig. 2d, and other images recorded for repeated experiments, the density of BDD nano-discs formed in the random array was determined to be 650 ± 25 million nano-discs per cm^2.

The cyclic voltammetric response of the RAN BDD electrode was recorded in the same solution as that used for the bare, nanoparticles and polymer modified electrodes to avoid any slight changes in the concentration of the solution. Fig. 1d shows the voltammetric response of the RAN BDD at 100 mV s^{-1} compared to the voltammetric response at the bare electrode. It is immediately apparent that by dissolving the MoO_2 nanoparticles we have restored the electroactivity of this electrode, indicating that the dissolution of the nanoparticles also removed the polymer immediately above them. The voltammetry remains characteristic of a system under diffusion control; even at slow scan rates 10 mV s^{-1} The peak-to-peak separation, observed in the voltammetry of ferrocyanide at the RAN BDD electrode, has increased slightly compared with the bare BDD macroelectrode, as expected if the RAN BDD electrode is exhibiting some vestigial degree of convergent diffusion. What is immediately apparent is that the RAN BDD array exhibits a much larger peak current than that of the bare BDD electrode. This is discussed in detail in Section 4 below.

The entire procedure described above was repeated several times to construct various RAN BDD electrodes. The resulting voltammetric response and distribution of sizes of the RAN BDD electrodes (20 ± 10 nm; average disc size for three separate RAN BDD electrodes was 18.6, 21.4 and 17.2 nm) was found to be reproducible and consistent within the limits reported. The number density varied slightly between different electrode surfaces due to the differing heterogeneity of each surface. However, the voltammetric response is similar in all cases.

It is apparent that the RAN BDD array is not exhibiting full diffusional independence. Davies et al. [5] have categorized the voltammetric behaviour at a given scan rate of random electrode arrays into four main categories corresponding to: type I: arrays of electrodes where diffusion to each element in the array is fully independent of its neighbouring elements and the diffusion to each element is planar; type II: arrays of electrodes where there are convergent diffusion layers at the different independent electrodes in the array; type III: similar to type II except that there is partial overlap between adjacent diffusion layers surrounding each element in the array. Diffusion to a type III array increasingly exhibits the characteristics of planar diffusion to the array as a whole whilst still retaining some convergent diffusion characteristics; type IV: an array of electrodes where there is full overlap of adjacent diffusion layers such that diffusion to the electrode surface can be considered to be planar. Types II, III and IV are similar to cases (b), (c) and (d), respectively, in Scheme 1. Fig. 4a and b show the voltammetry obtained at a RAN BDD array in 1 mM ferrocyanide solution at scan rates of 200 and 1000 m Vs^{-1}, respectively. At low scan rates the RAN-BDD exhibits voltammetry that is almost identical to that expected for a macrodisc electrode under linear diffusion except that the peak-to-peak separation for the RAN BDD electrode is slightly larger than for the bare BDD electrode, indicative of type III/IV behavior. From Fig. 4a and b we can observe that as the scan rate increases the RAN BDD array switches to type II/III behavior. This is evidenced by an increased peak separation, a larger post-peak current on the oxidative wave than that expected for planar diffusion alone and the shape of the wave changing from

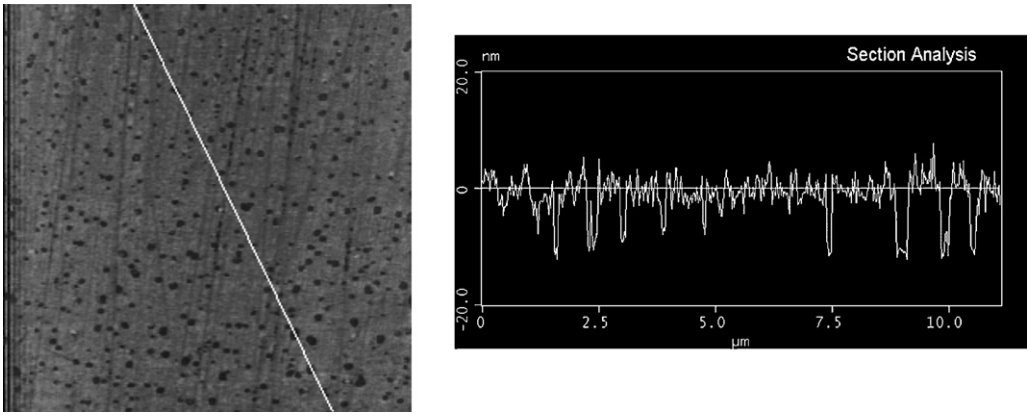

Fig. 3. The 2D AFM image of the RAN BDD electrode surface showing the corresponding line segment analysis across several BDD nano-discs.

peak-shaped to a more sigmoidal shape as the contribution of convergent diffusion to the array increases with increasing scan rate.

The capacitive charging at the bare BDD and a RAN BDD electrode was compared by cycling the potential in 0.1 M KCl over a range of scan rates (10 mV s^{-1} to 10 V s^{-1}). In all cases the capacitive charging (background) current was significantly reduced at the RAN BDD electrode compared to the bare BDD macrodisc electrode of the same geometric area. For example the charging current measured at 0 V for the bare array was 2.3×10^{-7} A whilst at the RAN BDD electrode the charging current was reduced by almost a quarter at 7.8×10^{-8} A. The reduction in background charging current offers a further analytical advantage of using the RAN BDD array for electroanalysis, particularly of trace analytes where often the Faradaic current responses of interest are obscured by the larger background charging currents.

4. Numerical simulation

In order to understand the voltammetric behavior of the BDD electrode, numerical simulations were performed of diffusion to a nano-disc array. The model used for simulation of a microdisc array has been described in detail previously [5,47]. The same approach is suitable here for modeling the current at the BDD electrode, although the discs have much smaller radius and distance of separation than the microdiscs previously considered. The array is treated approximately as a regular distribution and rigorously as a random distribution of nano-discs, and the simulated results are compared with the experimentally measured voltammetry.

4.1. Mathematical model

The array is divided up into cells, each one containing a single disc. The boundaries of these cells are chosen such that each cell is diffusionally independent, and so may be simulated separately. The diffusion domain approximation is applied, which treats each cell as being cylindrical. With cylindrical symmetry, the complex three-dimensional problem is reduced to two dimensions [5].

For a regular array, these diffusion domains are all equal in size. The total current measured at the array is found by simulating just one of the cells and then multiplying by the total number of discs present. For a randomly distributed array, the sizes of the diffusion domains are described by the following probability

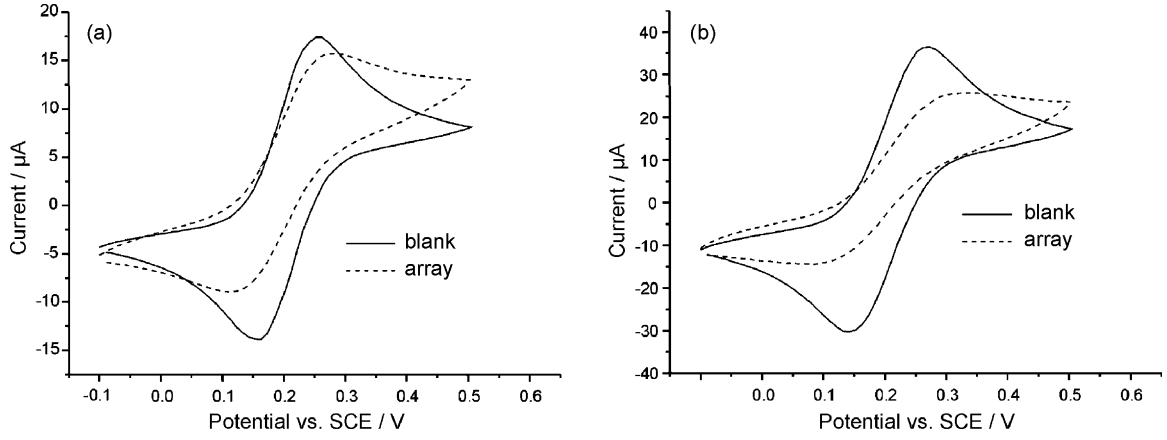

Fig. 4. The cyclic voltammetric response of both a bare BDD and a RAN BDD array in a 1.0 mM solution of potassium ferrocyanide at (a) 200 mV s^{-1} and (b) 1000 mV s^{-1} showing the switch between the different types of diffusional behavior (see text).

distribution function [48]:

$$P(S) = \frac{343}{15}\sqrt{\frac{7}{2\pi}}\left(\frac{S}{\langle S\rangle}\right)^{5/2}\exp\left(-\frac{7}{2}\frac{S}{\langle S\rangle}\right) \quad (3)$$

where S is the area of the diffusion domain and $\langle S\rangle$ is the average area. The current response of a randomly distributed disc array is found by simulating diffusion domains of a range of sizes, weighting the result by Eq. (3) and then multiplying by the total number of discs in the array.

The reaction at the electrode is modeled as the simple one electron reduction in Eq. (5). The concentration profile of species A is found for each diffusion domain by solving Fick's second law using a cylindrical coordinate system:

$$\frac{\partial[\mathrm{A}]}{\partial t} = D\nabla^2[\mathrm{A}] \quad (4)$$

It is assumed that both species have equal diffusion coefficients, such that the concentration profile of species A may be calculated independently of species B. It is assumed that the electron transfer is fast and reversible such that the ratio of A to B at the electrode surface is described by the Nernstian boundary condition in Eq. (6).

$$\mathrm{A} + \mathrm{e}^- \rightleftharpoons \mathrm{B} \quad (5)$$

$$\frac{[\mathrm{A}]_{\mathrm{elec}}}{[\mathrm{B}]_{\mathrm{elec}}} = \exp\left(\frac{F}{RT}(E - E_{\mathrm{f}}^{\mathrm{o}})\right) \quad (6)$$

The systems of linear equations generated by Eq. (4) are discretised by a finite difference method over an expanding rectangular grid. They are solved by the alternating direction implicit method using the Thomas algorithm.

4.2. Comparison of simulated and experimental data

The array was simulated using a disc radius of 10 nm, the value inferred from AFM imaging of the BDD electrode. Fig. 5 shows simulated voltammetry treating the array as a regular distribution with varying electrode densities. It is seen that as the electrode density increases, the peak current tends towards the Randles-Ševčík value but never exceeds it.

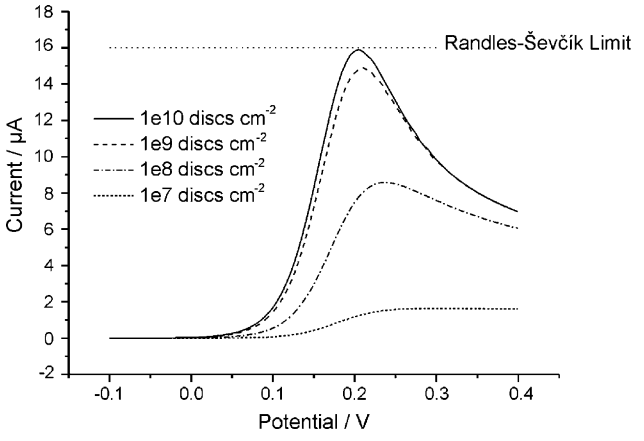

Fig. 5. Numerically simulated voltammograms for a regular array of nano-disc electrodes (radius = 10 nm) with varying numbers of electrode discs per unit area at a scan rate of 100 mV s^{-1} in 1.0 mM potassium ferrocyanide.

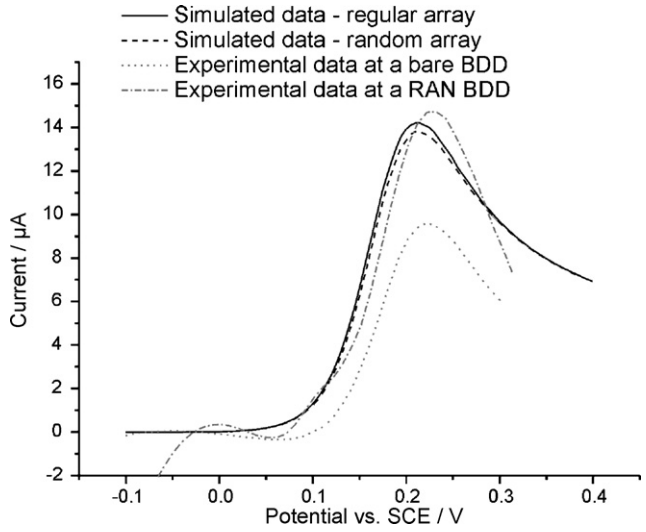

Fig. 6. A comparison between the baseline corrected experimental data recorded at a bare BDD electrode and a RAN BDD electrode in 1.0 mM potassium ferrocyanide at a scan rate of 100 mV s^{-1}, and numerical simulations of a regular and random array of 10 nm radius nano-disc electrodes using an electrode density of 650 million nano-discs per cm^2 over the same geometric area as the bare BDD electrode under the same experimental conditions. The experimental data shows only the forward sweep for clarity.

The BDD electrode was simulated using an electrode density of 650 million discs per cm^2, the value estimated from the AFM imaging. The array was treated as both a regular distribution and as a random distribution. Fig. 6 shows the agreement between the baseline corrected experimental data and the simulated data. Note that initially we included the recession of the BDD nano-discs within the polymer layer into the simulation model. However, this was found to have little effect on the simulated voltammetry for either the random or regular array and was therefore omitted from the simulation model shown here for reasons of simplicity and computational efficiency.

It is apparent that: (a) the peak current obtained at the RAN BDD array is close to the Randles-Ševčík limit for the geometric area of the array (type III/IV behavior) and that (b) that the bare BDD macrodisc electrode produces peak currents which are significantly less than that predicted by the Randles-Ševčík limit. In short the RAN BDD electrode exhibits currents that are significantly larger than those generated using the geometric area of the bare macroelectrode, despite most of the surface of the RAN BDD electrode being covered by electroinactive polymer. In fact the peak currents at the RAN BDD are almost 1.5 times as large as those at the bare electrode! To ensure that this effect was not simply due to the changes in the structure of the polymer layer upon contact with the acid solution, a control experiment was performed whereby the polymer layer was deposited on a bare BDD electrode in the absence of any MoO_2 nanoparticles, and then exposed to the dilute HCl solution as before. In this case the voltammetry remained identical to that in Fig. 1c, indicating that the polymer layer still effectively insulated the electrode, and that the restoration of the voltammetric response in Fig. 1d is indeed due to the removal of the MoO_2 nanoparticles to create the RAN BDD electrode. There is a small shoulder on the oxidative wave in Fig. 1d which might possibly be attributable

to a small amount of ferrocyanide trapped within the polymer layer.

5. Conclusions

Random arrays consisting of 650 ± 25 million BDD disc electrodes per cm^2, 20 ± 10 nm in diameter have been constructed using a facile three-step procedure. The electrode is characterized at each stage of the manufacturing process using cyclic voltammetry over the scan range of 10–10,000 $mV\,s^{-1}$ and AFM imaging. Not only is this the first such array of nanometer sized BDD electrodes reported, but the capacitive charging currents at the RAN BDD array are significantly reduced compared to a bare BDD macrodisc, recovering the maximum possible peak current predicted by the Randles-Ševčík equation. We believe that the RAN BDD electrode proffers significant benefits to the electroanalytical determination of a wide range of important analytes.

Acknowledgements

LX thanks the EPSRC and Windsor Scientific for an Industrial CASE award. IS thanks the EPSRC for a DTA award. GGW thanks St. John's College, Oxford, for a Junior Research Fellowship.

References

[1] T.S. Harrison, Who discovered microelectrodes, J. Hist. Neurosci. 9 (2000) 165.
[2] A.J. Bard, L.R. Faulkner, Electrochemical Methods, Fundamentals and Applications, 2nd edition, John Wiley & Sons Inc., New York, 2001.
[3] T.J. Davies, B.A. Brookes, R.G. Compton, A computational and experimental study of the cyclic voltammetry response of partially blocked electrodes. Part III: Interfacial liquid-liquid kinetics of aqueous vitamin B12s with random arrays of femtolitre microdroplets of dibromocyclohexane, J. Electroanal. Chem. 566 (2004) 193–216.
[4] T.J. Davies, B.A. Brookes, A.C. Fisher, K. Yunus, S.J. Wilkins, P.R. Greene, J.D. Wadhawan, R.G. Compton, A computational and experimental study of the cyclic voltammetry response of partially blocked electrodes. Part II: Randomly distributed and overlapping blocking systems, J. Phys. Chem. B 107 (2003) 6431–6444.
[5] T.J. Davies, S. Ward-Jones, C.E. Banks, J. Del Campo, R. Mas, F.X. Munoz, R.G. Compton, The cyclic and linear sweep voltammetry of regular arrays of microdisc electrodes: fitting of experimental data, J. Electroanal. Chem. 585 (2005) 51–62.
[6] T.J. Davies, C.E. Banks, R.G. Compton, J. Solid State Electrochem. 9 (2005) 797.
[7] K. Aoki, J. Osteryoung, Diffusional inpdependence criteria, J. Electroanal. Chem. 125 (1981) 315.
[8] W.L. Caudill, J.O. Howell, R.M. Wightman, Diffusional independence criteria, Anal. Chem. 54 (1982) 2532.
[9] A.O. Simm, S. Ward-Jones, C.E. Banks, R.G. Compton, Novel methods for the production of silver microelectrode-arrays: their characterisation by atomic force microscopy and application to the electroreduction of halothane, Anal. Sci. 21 (2005) 667–671.
[10] C.M. Welch, R.G. Compton, The use of nanoparticles in electroanalysis: a review, Anal. Bioanal. Chem. 384 (2006) 601–619.
[11] Y.H. Lanyon, D.W.M. Arrigan, Recessed nanoband electrodes fabricated by focused ion beam milling, Sens. Actuators B 121 (2007) 341.
[12] Y.H. Lanyon, G. De Marzi, Y.E. Watson, A.J. Quinn, J.P. Gleeson, G. Redmond, D.W.M. Arrigan, Fabrication of nanopore array electrodes by focused ion beam milling, Anal. Chem. 79 (2007) 3048.
[13] M.E. Sandison, J.M. Cooper, Nanofabrication of electrode arrays by electron-beam lithography and nanoimprint lithographies, Lab. Chip 8 (2006) 1020.
[14] O. Ordeig, C.E. Banks, T.J. Davies, J. del Campo, R. Mas, F.X. Munoz, R.G. Compton, Regular arrays of microdisc electrodes: simulation quantifies the fraction of 'dead' electrodes, Analyst 131 (2006) 440–445.
[15] J.O. Besenhard, A. Schulte, K. Schur, P.D. Jannakoudakis, Carbon fibre microelectrodes, NATO ASI Series E, Appl. Sci. 197 (1991) 189.
[16] O. Niwa, Carbo nanostructured film based microelectrodes, Bull. Chem. Soc. Japan 78 (2005) 555.
[17] S. Fletcher, M.D. Horne, Random assemblies of microelectrodes (RAM electrodes) for electrochemical studies, Electrochem. Commun. 1 (1999) 502–512.
[18] O. Ordeig, C.E. Banks, T.J. Davies, J. del Campo, F.X. Munoz, R.G. Compton, The linear sweep voltammetry of random arrays of microdisc electrodes: fitting of experimental data, J. Electroanal. Chem. 592 (2006) 126–130.
[19] D.A. Fungaro, C.M.A. Brett, Microelectrode arrays: application in batch-injection analysis, Anal. Chim. Acta 385 (1999) 257–264.
[20] L.J. Cain, Metal ion analysis by diffusional microtitration: electrochemical generation of EDTA at carbon-fiber microelectrode arrays, Diss. Abstr. Int. B 59 (1998) 195.
[21] Y. Guo, M. Shao, C. Zhang, J. Zhao, Determination of neurotransmitter in body fluid with voltammetry at bevelled carbon fiber array electrodes, Fenxi Huaxue 25 (1997) 527–530.
[22] M. Armstrong-James, J. Millar, Carbon fibre microelectrodes, J. Neurosci. Methods 1 (1979) 279–287.
[23] J.M. Pingarron, P. Yanez-Sedeno Orive, Trends in Electrochemistry and Corosion at the Beginning of the 21st Century, University of Barcelona, Barcelona, 2004.
[24] I. Ivanov, A. Puretzky, G. Eres, H. Wang, Z. Pan, H. Cui, R. Jin, J. Howe, D.B. Geohegan, Fast and highly anisotropic thermal transport through vertically aligned carbon nanotube arrays, Appl. Phys. Lett. 89 (2006), 223110/223111–223110/223113.
[25] J.-S. Ye, Y. Wen, W.-D. Zhang, H.F. Cui, G.Q. Xu, F.-S. Sheu, Electrochemical functionalization of vertically aligned carbon nanotube arrays with molybdenum oxides for the development of a surface-charge-controlled sensor, Nanotechnology 17 (2006) 3994–4001.
[26] H. Wang, Z. Xu, G. Eres, Order in vertically aligned carbon nanotube arrays, Appl. Phys. Lett. 88 (2006), 213111/213111–213111/213113.
[27] X.R. Ye, L.H. Chen, C. Wang, J.F. Aubuchon, I.C. Chen, A.I. Gapin, J.B. Talbot, S. Jin, Electrochemical modification of vertically aligned carbon nanotube arrays, J. Phys. Chem. B 110 (2006) 12938–12942.
[28] S.J. Shin, D.-W. Choi, H.-S. Kwak, G.I. Lim, Y.S. Choi, Matrix-free laser desorption/ionization on vertically aligned carbon nanotube arrays, Bull. Kor. Chem. Soc. 27 (2006) 581–583.
[29] R. Zheng, G.A. Cheng, Y. Peng, Y. Zhao, H. Liu, C. Liang, Synthesis of vertically aligned carbon nanotube arrays on silicon substrates, Sci. Chin. Ser. E: Eng. Mater. Sci. 47 (2004) 616–624.
[30] http://www.nano-lab.com/home.html.
[31] J. Li, J.E. Koehne, A.M. Cassell, H. Chen, H.T. Ng, Q. Ye, W. Fan, J. Han, M. Meyyappan, Inlaid multi-walled carbon nanotube nanoelectrode arrays for electroanalysis, Electroanalysis 17 (2005) 15–27.
[32] J. Koehne, J. Li, A.M. Cassell, H. Chen, Q. Ye, H.T. Ng, J. Han, M. Meyyappan, The fabrication and electrochemical characterization of carbon nanotube nanoelectrode arrays, J. Mater. Chem. 14 (2004) 676–684.
[33] J. Li, H.T. Ng, A. Cassell, W. Fan, H. Chen, Q. Ye, J. Koehne, J. Han, M. Meyyappan, Carbon nanotube nanoelectrode array for ultrasensitive DNA detection, Nano Lett. 3 (2003) 597–602.
[34] A.O. Simm, C.E. Banks, S. Ward-Jones, T.J. Davies, N.S. Lawrence, T.G.J. Jones, L. Jiang, R.G. Compton, Boron-doped diamond microdisc arrays: electrochemical characterisation and their use as a substrate for the production of microelectrode arrays of diverse metals (Ag, Au, Cu) via electrodeposition, Analyst 130 (2005) 1303–1311.

[35] A.P. O'Mullane, A.K. Neufeld, A.R. Harris, A.M. Bond, Electrocrystallization of phase I, CuTCNQ (TCNQ = 7,7,8,8-Tetracyanoquinodimethane), on indium tin oxide and boron-doped diamond electrodes, Langmuir 22 (2006) 10499–10505.
[36] K. Tsunozaki, Y. Einaga, T.N. Rao, A. Fujishima, BDD microarray, Chem. Lett. 5 (2002) 502.
[37] C. Provent, W. Haenni, E. Santoli, P. Rychen, BDD microarray, Electrochim. Acta 49 (2004) 3737.
[38] K.L. Soh, W.P. Kang, J.L. Davidson, S. Basu, Y.M. Wong, D.E. Cliffel, A.B. Bonds, G.M. Swain, BDD microarrays, Diamond Relat. Mater. 13 (2004) 2009.
[39] C. Madore, A. Duret, W. Haenni, A. Perret, BDD microarray, Proc. Electrochem. Soc. 159 (2000) 2000–2019.
[40] M.E. Hyde, T.J. Davies, R.G. Compton, Fabrication of random assemblies of metal nanobands: a general method, Angew. Chem. Int. Ed. 44 (2005) 6491–6496.
[41] T.J. Davies, M.E. Hyde, R.G. Compton, Nanotrench arrays reveal insight into graphite electrochemistry, Angew. Chem. Int. Ed. 44 (2005) 5121–5126.
[42] M.P. Zach, K. Inazu, K.H. Ng, J.C. Hemminger, R.M. Penner, Synthesis of molybdenum nanowires with millimeter-scale lengths using electrochemical step edge decoration, Chem. Mater. 14 (2002) 3206–3216.
[43] M.P. Zach, K.H. Ng, R.M. Penner, Molybdenum nanowires by electrodeposition, Science 290 (2000) 2120–2123.
[44] K. Jurkschat, S.J. Wilkins, C.J. Salter, H.C. Leventis, G.G. Wildgoose, L. Jiang, T.G.J. Jones, A. Crossley, R.G. Compton, Multiwalled carbon nanotubes with molybdenum dioxide nanoplugs—new chemical nanoarchitectures by electrochemical modification, Small 2 (2006) 95–98.
[45] F.G. Chevallier, T.J. Davies, O.V. Klymenko, L. Jiang, T.G.J. Jones, R.G. Compton, Numerical simulation of partially blocked electrodes under cyclic voltammetry conditions: influence of the block unit geometry on the global electrochemical properties, J. Electroanal. Chem. 577 (2005) 211–221.
[46] B.A. Brookes, T.J. Davies, A.C. Fisher, R.G. Evans, S.J. Wilkins, K. Yunus, J.D. Wadhawan, R.G. Compton, Computational and experimental study of the cyclic voltammetry response of partially blocked electrodes. Part 1. Nonoverlapping, uniformly distributed blocking systems, J. Phys. Chem. B 107 (2003) 1616–1627.
[47] F.G. Chevallier, R.G. Compton, Regular arrays of microdisk electrodes: numerical simulation as an optimizing tool to maximize the current response and minimize the electrode area used, Electroanalysis 18 (2006) 2369–2374.
[48] F. Járai-Szabó, Z. Néda, On the size-distribution of Poisson Voronoi cells, arXiv Condens. Matter e-prints 06 (2004) 116.

Biographies

Lei Xiao is a postgraduate student, currently working on nanomaterials for electroanalysis in St John's College Oxford. He completed MChem in Chemistry in Somerville College, Oxford University.

Ian Streeter is a DPhil student at Oxford University studying computational electrochemistry.

Gregory G. Wildgoose completed his MChem and DPhil in 2003 and 2006 respectively at Oxford University. In 2006, he was elected as a Junior Research Fellow at St John's College, Oxford. He has published over 50 papers and is a referee for several international journals. He has broad interests in electrochemistry and electroanalysis in conjunction with other surface analysis techniques such as XPS, AFM etc. Currently he is focussed on studying the underlying physicochemical processes occurring carbon-based electrodes and at nanoscale materials such as carbon nanotubes and inorganic nanomaterials and also their chemical modification with a range of organic and inorganic species with an aim to developing practical applications for these novel materials.

Richard G. Compton is a Professor of Chemistry at Oxford University and Tutor in Chemistry at St John's College. He is Editor-in-Chief of the journal Electrochemistry Communications and has published over 800 papers and reviews in refereed journals. He has broad interests in electrochemistry and electroanalysis.